

AperTO - Archivio Istituzionale Open Access dell'Università di Torino

Ultrahigh-pressure metamorphism in the magnesite + aragonite stability field: evidence from two impure marbles from the Dabie-Sulu UHPM belt.

This is the author's manuscript

Original Citation:

Availability:

This version is available <http://hdl.handle.net/2318/120303> since

Published version:

DOI:10.1111/jmg.12005

Terms of use:

Open Access

Anyone can freely access the full text of works made available as "Open Access". Works made available under a Creative Commons license can be used according to the terms and conditions of said license. Use of all other works requires consent of the right holder (author or publisher) if not exempted from copyright protection by the applicable law.

(Article begins on next page)



UNIVERSITÀ DEGLI STUDI DI TORINO

This is an author version of the contribution published on:

Proyer A., Rolfo F., Zhu Y.F., Castelli D., Compagnoni R.
Ultrahigh-pressure metamorphism in the magnesite + aragonite stability field:
evidence from two impure marbles from the Dabie-Sulu UHPM belt.
JOURNAL OF METAMORPHIC GEOLOGY (2013) 31
DOI: 10.1111/jmg.12005

The definitive version is available at:
<http://doi.wiley.com/10.1111/jmg.12005>

1 **Ultrahigh-pressure metamorphism in the magnesite + aragonite stability**
2 **field: evidence from two impure marbles from the Dabie-Sulu UHPM belt.**

3

4 ALEXANDER PROYER^{1*}, FRANCO ROLFO², YONG-FENG ZHU³, DANIELE CASTELLI²,
5 ROBERTO COMPAGNONI²

6

7 ¹ University of Graz, Universitaetsplatz 2/II, 8010 Graz, Austria;

8 *Corresponding author, e-mail: alexander.proyer@uni-graz.at

9 ²University of Torino, Via Valperga Caluso 35,10135 Torino, Italy

10 ³Peking University, Beijing 100871, China

11

12

13 Short title: UHPM in the magnesite + aragonite stability field

14 **ABSTRACT**

15

16 Two magnesite-bearing impure dolomitic marbles from the Dabie-Sulu UHP region have
17 been investigated in order to clarify if they had actually attained *P-T* conditions outside the
18 dolomite stability field, limited by the reaction dolomite = aragonite + magnesite, and to test
19 their potential for recording (U)HP conditions. In both cases the silicate mineral assemblage
20 records conditions around the terminal amphibole breakdown reaction: amphibole + aragonite
21 ± quartz = clinopyroxene + talc, which is a good geobarometer between at least 2.0 and 2.6
22 GPa. At higher pressures, the terminal breakdown of talc to clinopyroxene + coesite is
23 another *P-T* milestone that can be inferred from possible pseudomorphs of talc + calcite after
24 coesite, at least in one sample. The dolomite dissociation curve becomes strongly divariant in
25 Fe-bearing marbles and may be attainable during cold subduction near the 5°C/km
26 “geotherm”. At least one of the samples (from Xinyan village, near Taihu, Dabie Shan)
27 preserved relics of both magnesite and aragonite and most likely attained conditions within
28 the aragonite + magnesite stability field. For the second sample from Sanqingge village in the
29 Sulu terrane no certain evidence has been found in this study. Impure dolomitic marbles have
30 considerable potential to preserve (ultra)high-pressure relics, and the inconspicuous mineral
31 assemblage clinopyroxene + talc or quartz (after former coesite) may in fact record UHP
32 conditions.

33

34 Keywords: UHP metamorphism, dolomite dissociation, magnesite, aragonite, Dabie-Sulu

35

36 INTRODUCTION

37

38 The mineral assemblage magnesite + aragonite is of considerable interest for researchers
39 dealing with ultrahigh-pressure (UHP) metamorphism, crust-mantle interaction or carbonate
40 stability in the upper mantle because the breakdown of dolomite to magnesite + aragonite has
41 been determined in a series of experiments (Liu & Lin, 1995; Martinez *et al.*, 1996; Luth,
42 2001; Sato & Katsura, 2001; Buob *et al.*, 2006; Morlidge *et al.*, 2006) to occur at very high
43 pressures, within the so-called “forbidden zone”, i.e. at “geothermal gradients” below 5°C per
44 km (Fig. 1). Even though there is a considerable spread between the different experimental
45 results, search for traces indicating the (former) presence of a magnesite + aragonite bearing
46 mineral assemblage in ultrahigh-pressure marbles or eclogites is indicated because the
47 number of possible geothermobarometers in that P - T range is very limited and the tectonic
48 consequences of such finds quite important.

49

50 Although dolomitic marbles can be found in almost any UHP metamorphic area with
51 metamorphosed supracrustal rocks, only Zhu & Ogasawara (2002) and Zhu (2005) reported
52 observation of dolomite decomposition in marbles from Kokchetav and from the Sulu-terrane
53 in China, but these observations were contested (Hermann, 2003; Zhu, 2003) or revised after
54 a more detailed investigation (Zhu *et al.*, 2009) to the effect that the dolomite-magnesite
55 marble investigated had not crossed the dolomite-out curve. Omori *et al.* (1999) discovered
56 rare magnesite in impure dolomitic marbles from Xinyan (Dabie Shan) and concluded from
57 the apparent textural disequilibrium of calcite-magnesite intergrowths that this rock also had
58 not experienced pressures above the dolomite dissociation curve. Liu *et al.* (2006) however
59 claim from inclusions of both aragonite and magnesite in the same “UHP growth zone” in

60 zircon that these marbles had passed the dolomite-out curve during their metamorphic
61 history.

62

63 Carbonate-bearing eclogites and metapelites from Dabie Shan and Tian Shan in China
64 however are reported to fulfill the requirements: Zhang & Liou (1996) describe a dolomite-
65 magnesite-bearing coesite-eclogite that also contains calcite-pseudomorphs after former
66 aragonite as inclusions in garnet, and Zhang *et al.* (2003) observed inclusions of magnesite
67 and calcite (interpreted as pseudomorphs after former aragonite) in large dolomite
68 porphyroblasts in a garnet-chloritoid-glaucophane micaschist. In both cases, a former
69 coexistence of magnesite and aragonite was inferred. Only one carbonate mineral is stable at
70 a time, however, in the majority of carbonate-bearing metabasites, with a reported change
71 with increasing pressure from aragonite to dolomite to magnesite-bearing blueschists and
72 eclogites (e.g. Messiga *et al.*, 1999; Zhang *et al.*, 2003).

73

74 The present study is a detailed investigation of magnesite-bearing dolomitic marbles sampled
75 from the same localities as those of Omori *et al.* (1999) and Zhu *et al.* (2009) with the
76 purpose of understanding the complex calcite-dolomite-magnesite intergrowth
77 microstructures in order to establish whether the dolomite dissociation curve had actually
78 been overstepped at some point of the metamorphic history of these rocks.

79

80 **SAMPLE LOCATIONS**

81

82 The first sample of impure dolomitic marble (RPC-159) was taken from a river profile near
83 Xinyan, less than 2 km from the well known Shima gneiss+eclogite and Maowu garnet-
84 peridotite in the Coesite Eclogite Complex of eastern Dabie Shan. The local geology,

85 lithologies and metamorphic history as derived mainly from eclogites have been described in
86 Zhang & Liou (1996), Omori *et al.* (1999), Oberhänsli *et al.* (2002), Schmid *et al.* (2000,
87 2003) and Rolfo *et al.* (2004) and will not be covered here.

88 The second sample (XU-1) was collected in a quarry ca. 1 km northeast of the village of
89 Sanqingge in the Sulu terrane. The location and its geological inventory are described in
90 detail in Zhu *et al.* (2009). Folded bands of mostly dolomitic marble are separated by thin
91 layers of eclogite, and three different types of marble, depending on the degree of
92 retrogression, have been distinguished (Zhu *et al.*, 2009). The sample used for this study
93 belongs to the least retrogressed magnesite marble type and was taken directly from the
94 contact with an eclogite layer.

95

96 **PETROGRAPHY**

97

98 **Sample RPC-159**

99 This is a dolomite marble that contains large porphyroblasts of omphacite and tremolite (Fig.
100 2a) together with subordinate calcite and the accessory minerals epidote, zircon, rutile,
101 apatite, pyrrhotite and chalcopyrite. Quartz is found only as inclusions in tremolite or at grain
102 boundaries between tremolite and omphacite, magnesite as inclusions in dolomite and tiny
103 relics of talc are rarely preserved in matrix dolomite (Fig. 2b). Omphacite and tremolite
104 porphyroblasts are xenomorphic, with no apparent compositional zoning in spite of their
105 large grain sizes of up to several millimeters. Epidote can be found both as inclusions and in
106 the rock matrix and shows oscillatory zoning with local enrichment in Ce and Fe³⁺ (Fig. 2c).
107 The degree of retrogression is minor: omphacite decomposes into a fine- to medium-grained
108 symplectite of diopside + tremolite + albite ± calcite (Fig. 2d). Rutile affected by such
109 alteration zones is partly replaced by titanite (Fig. 2e). The symplectites around phengitic

110 muscovite consist of Ba-rich muscovite + phlogopite + albite (Fig. 2f). Rounded inclusions of
111 microcrystalline talc + calcite in omphacite, surrounded by cracks could be pseudomorphs
112 after former coesite (Fig. 2g). Apatite cores are strewn with micrometer-sized blebs and
113 needles of a Ce-rich phosphate – presumably monazite. The needles are crystallographically
114 oriented in at least three different directions, indicating a precipitate origin (Fig. 2h).

115

116 The most revelatory mineral microstructures are those of the carbonate phases. Magnesite has
117 yet been found only as inclusions in dolomite, but its degree of preservation can vary from
118 completely fresh, often oval grains with straight grain boundaries to completely replaced by a
119 porous type of calcite with or without additional dolomite or a Mg-Si-bearing talc-like
120 mineral, which is, however, too poorly crystallized for a reasonable microprobe
121 measurement. The various states of replacement are documented in Figs 3a-d.

122 Calcite occurs in three different morphological varieties. Pseudomorphic replacement of
123 magnesite invariably results in a porous type of calcite (Fig. 3d). Another type of matrix
124 calcite contains abundant blebs of dolomite and is interpreted as former high-Mg-calcite (Fig.
125 3e). Some, but not all of these calcite grains are found as part of medium grained amphibole
126 + quartz or symplectite replacement microstructures after omphacite, and could be by-
127 products of the omphacite breakdown reaction. A third type of calcite is devoid of pores and
128 of dolomite inclusions. It was observed mainly as inclusions in omphacite, often with
129 concentric cracks, and more rarely included in dolomite or adjacent to omphacite or dolomite
130 grains (Figs 3f,g). One such grain contains relics of a BSE-brighter CaCO_3 mineral, which is
131 aragonite (Fig. 3g), as verified by Raman spectra which show a peak at 206 wavenumbers
132 which is typical for aragonite and absent in calcite. The Mg-content of the latter calcites is
133 negligible (see below), consequently these grains are considered to represent former aragonite

134 as well. Finally, BSE-imaging revealed dolomite within dolomite, i.e. a grain of dolomite
135 with a brighter BSE-contrast than the surrounding “normal” matrix dolomite (Fig. 3h).

136

137 **Sample XU-1**

138 The thin section of sample XU-1 goes right across the contact between eclogite and dolomitic
139 marble, which are separated by a thin monomineralic band of amphibole 2-3 mm across. The
140 eclogite consists mainly of omphacite and subordinate garnet, phengite and rutile, which are
141 rimmed or replaced respectively by: symplectites of amphibole + plagioclase, Fe-Al-rich
142 amphibole, symplectites of biotite + plagioclase, and titanite. The marble is composed of
143 dolomite, calcite, amphibole, talc and very minor chlorite (Fig. 4a). Both tremolite and talc
144 are coarse-grained (up to mm-sized). Talc is inclusion-free whereas tremolite often contains
145 inclusions of quartz and more rarely of omphacite, magnesite and calcite. Omphacite is not
146 stable in the matrix but was replaced by amphibole + quartz (Fig. 4f). The quartz inclusions
147 in amphibole are sometimes fresh, but more often develop reaction coronas of talc plus
148 calcite (Fig. 4b). Dolomite also contains inclusions of omphacite, magnesite and amphibole
149 and shows a complex chemical zoning with BSE-darker cores and brighter peripheral parts
150 (Figs 4c,g). The degree of brightness increases with Fe-content of dolomite, the source of
151 which, in some cases at least, seems to be inclusions of relict magnesite (Figs 4c,e).

152

153 Calcite is modally dominant over magnesite in the matrix, where the former replaces the
154 latter (Fig. 4d) and displays a variety of microstructures, the most common one being non-
155 porous calcite along former grain margins of magnesite and polycrystalline porous calcite
156 towards the centers of such pseudomorphic replacement microstructures (Fig. 5a). However,
157 a non-porous calcite and a mixed type also exist (Figs 5b-d), sometimes with a BSE-zoning
158 due to variable Fe-content, and even a calcite type with complex zoning has been observed

159 (Figs 5e,f). Finally, a fourth textural type of calcite is filling abundant cracks in dolomite
160 (Fig. 4a). In contrast to sample RPC159, a BSE-bright substance is part of the pseudomorphs.
161 The EDX spectra show predominant Fe and subordinate Si in variable proportions; analytical
162 totals vary largely between 65 and 80 wt%, indicating significant porosity and most likely
163 also the presence of undetected light elements. A tentative identification by Raman
164 spectroscopy points to a combination of goethite + amorphous silica as the most likely
165 constituents. Concentrations of this BSE-bright material often run parallel to former grain
166 boundaries of magnesite between porous and non porous calcite of the pseudomorphs (Figs
167 4d,g). Xenoblastic magnesite is very often preserved in the centers of such pseudomorphs.
168 Uncorroded magnesite is restricted to inclusions in amphibole and was found in one instance
169 as an inclusion in apatite (Figs 6a-c). Compositional zoning of magnesite and dolomite is due
170 to variable Fe-Mg ratios (see below) and usually rather irregular or patchy and rarely
171 concentric, with more Fe-rich rims.

172

173 **MINERAL COMPOSITIONS**

174

175 Quantitative chemical analyses were obtained with a Superprobe JEOL JXA 8200 with 5
176 WDX spectrometers in the E.F. Stumpfl EMP-Laboratory, Leoben, and additionally with a
177 JEOL JSM 6310 scanning electron microscope equipped with an Oxford Link ISIS EDX
178 spectrometer and a Microspec WDX spectrometer at the University of Graz. Analytical
179 conditions were 15 kV accelerating voltage and 6 nA probe current for silicates and 2 nA for
180 carbonates respectively, with a 1-2 μ m diameter of the focused beam and counting times were
181 20-30 seconds on peak and 10-15 seconds on lower and upper background positions
182 respectively. Matrix correction of phi-rho-Z-type was performed with internal software.
183 Standards were adularia (K, Si), garnet (Fe, Mg), rhodonite (Mn), titanite (Ca, Ti), chromite

184 (Cr), gahnite (Zn) and jadeite (Na), and calcite (Ca), dolomite(Mg) and siderite (Fe, Mn) for
185 carbonate analyses. Mineral formulae and endmembers were calculated with the softwares
186 PET (Dachs, 1998, 2004) and AX (Holland, www.esc.cam.ac.uk/astaff/holland/), and mineral
187 chemical plots with PET or GCDkit (Janousek et al. 2006)

188

189 Representative mineral analyses for sample RPC-159 are given in Table 1. Large omphacite
190 grains are slightly zoned, with increasing Na, Al and Fe_{tot} and decreasing Ca and Mg from
191 core to rim (Fig. 7a). The composition range in terms of endmembers is about Di₆₉.
192 $_{75}\text{Hed}_2\text{Jd}_{15-20}\text{CaTs}_3\text{Aeg}_{2-5}$. Amphiboles are calcic to sodic-calcic (tremolite to winchite, Figs
193 7b,c) and display minor compositional zoning in Ca, Mg versus Na, Al, with all other
194 elements remaining constant. Muscovite contains up to 3.40 a.p.f.u. Si, is enriched in barium
195 also in its non-decomposed cores (up to 3.4 wt% or 0.68 a.p.f.u.) and contains a few Mol% of
196 paragonite, talc and pyrophyllite endmembers (Tab. 1). No fresh talc could be found in this
197 sample; the analyses in Table 1 are from a rounded talc-rich pseudomorph with radial cracks
198 in omphacite. Most noteworthy is the complete absence of Al and F.

199 Symplectite along cracks and rims of omphacite consists of Na-rich diopside, pure albite and
200 an amphibole that is significantly more tremolitic than coarse-grained matrix amphibole.

201 Magnesite without alteration rims of calcite is more magnesian $\text{Mg}_{91-93}\text{Fe}_{6-7}\text{Ca}_1$ and becomes
202 partly more ferroan during replacement: $\text{Mst}_{89-90}\text{Sid}_{8-9}\text{Cal}_1$ (Fig.8a). Matrix calcite is highest
203 in Mg- and Fe-content ($\text{Cal}_{94}\text{Mst}_{06}\text{Sid}_{01}$) – even without integrating dolomite exsolutions (Fig
204 8b). The non-porous calcite inclusions in omphacite range from entirely pure CaCO_3 to
205 $\text{Cal}_{97}\text{Mst}_{03}$. Calcite replacing magnesite ranges at the high-Mg end of these compositions. In
206 matrix dolomites, Ca correlates negatively with Mg, with a range of $\text{Cal}_{48-50}\text{Mst}_{47-49}\text{Sid}_{2-3}$,
207 whereby $(\text{Mg}+\text{Mn}+\text{Fe}) > \text{Ca}$ (Figs 8c,d). The BSE-brighter dolomite grains within a large
208 dolomite crystal are significantly richer in Ca, with $(\text{Mg}+\text{Mn}+\text{Fe}) < \text{Ca}$.

209

210 In sample XU-1 (Table 1) the amphiboles show subtle compositional zoning with barroisitic
211 cores and a trend to more tremolite-rich composition towards the rims (Fig. 7b). Within the
212 first centimeter from the eclogite contact there is no significant change in amphibole
213 composition as a function of distance. Omphacite inclusions are virtually pure ternary
214 diopside-hedenbergite-jadeite solid solutions (very low K, Fe^{3+} , $^{\text{IV}}\text{Al}$) and show a
215 considerable spread in jadeite component from 20 to 42 Mol% (Fig. 6a). The highest jadeite
216 content was found in an inclusion in quartz, followed by inclusions in dolomite and
217 amphibole, with the lowest values for inclusions in calcite (Table 1). The magnesite in
218 sample XU-1 has a slightly higher Fe/Mg ratio (less Ca) than that of sample RPC-159 (Fig.
219 8a), with a composition range of $\text{Mst}_{89-92}\text{Sid}_{7-11}\text{Cal}_1$. Porous and non-porous calcites from the
220 pseudomorphs are indistinguishable in terms of major element composition and cover most of
221 the compositional range of pseudomorphic and non-porous calcites of sample RPC-159 with
222 the exception of pure CaCO_3 compositions. Fe is slightly above and Mn below the detection
223 limit, Ca and Mg correlate well and range within $\text{Cal}_{97-100}\text{Mst}_{0-3}$ (Fig. 7b). Matrix dolomites
224 are less ferroan and thus higher in Mg compared to those in sample RPC-159 (Fig. 8c). The
225 conspicuous BSE-zoning of dolomites corresponds to a relatively narrow composition range
226 from pure $\text{Cal}_{50}\text{Mst}_{50}$ to $\text{Mst}_{48-49}\text{Sid}_{1-3}\text{Cal}_{48-50}$, whereby $(\text{Mg}+\text{Mn}+\text{Fe}) > \text{Ca}$ (Fig 8c, d). Mg is
227 inversely correlated with Fe+Mn, while Ca shows no correlation with any of the other
228 cations.

229

230 **DISCUSSION**

231

232 **Geothermobarometry and reaction history of the magnesite-bearing marbles**

233

234 A petrogenetic grid in the model system CaO-MgO-SiO₂-H₂O-CO₂ (CMSCH) was calculated
235 with THERMOCALC 3.3 (thermodynamic dataset from 22 Nov. 2003) for the P-T range of
236 1.5 – 4.5 GPa and 300 – 900°C to show the reactions that cause significant modal changes
237 (Fig. 9). Adding the components FeO, Al₂O₃ and Na₂O would increase the variance of these
238 equilibria in the natural samples and stabilize the corresponding assemblages over a larger *P*-
239 *T* range. In addition to the polymorphic phase transitions and the dolomite dissociation curve
240 in the upper left corner, the key feature of this diagram is the strongly pressure-dependent
241 degenerate reaction tremolite = diopside + talc, which passes through 4 invariant points. The
242 reactions, emanating from these points towards higher pressures into the UHP field, delimit
243 the stability field of talc in (1) aragonite-dolomite marbles, (2) dolomite-magnesite marbles
244 and (3) rocks with magnesite as the only carbonate mineral. Towards higher temperatures talc
245 breaks down to quartz/coesite + clinopyroxene or enstatite. Only the terminal breakdown
246 reaction of talc, emanating from invariant point (4) applies to ultrabasic compositions, while
247 the others are valid for quartz-saturated rocks. The coloured ellipses in Fig. 9 indicate *P-T*
248 estimates performed by prior workers.

249 We would first like to discuss the metamorphic history of the investigated marbles in this
250 framework and then compare the *P-T* estimates obtainable from them (using
251 THERMOCALC, mode average *PT*) with prior *P-T* estimates for these areas.

252

253 The observed mineral microstructures and compositions in sample RPC-159 can be explained
254 as follows: an aragonite-bearing dolomite marble passes into the omphacite + talc stability
255 field along the prograde subduction path, and subsequently crosses the dolomite
256 decomposition curve to become an aragonite-magnesite marble. During exhumation,
257 magnesite and aragonite mostly back-react to dolomite, leaving only isolated relics of
258 aragonite (in omphacite, dolomite and matrix) and magnesite (inclusions in dolomite).

259 During subsequent breakdown of omphacite + talc to amphibole \pm quartz all talc is consumed
260 (relics occurring only as rare and poorly preserved inclusions in omphacite and dolomite).
261 Quartz is clearly a reaction product and occurs only as part of this reaction microstructure,
262 generally included in amphibole. Aragonite later transforms to calcite. The coarse-grained
263 omphacite + tremolite assemblage is still largely preserved with the exception of partial
264 symplectite-type retrogression. The fine-grained, porous nature of the minerals
265 pseudomorphically replacing magnesite indicates low temperatures for this stage. The
266 dolomite-in-dolomite microstructure might indicate that at least some magnesite grains were
267 replaced earlier - in a process with different kinetics - by dolomite only.

268

269 Omori *et al.* (1999) had already observed the disequilibrium replacement microstructures of
270 magnesite by calcite but not differentiated between the different types of calcite, which
271 makes it possible to better understand the metamorphic evolution. They also observed
272 magnesite being replaced by an inner rim of dolomite and an outer rim of calcite (their Fig.
273 4b) – a microstructure that was not found in our study but that can be expected and may
274 represent a transitional type to the dolomite-in-dolomite microstructure reported here.

275

276 As indicated by the blue ellipses in Fig. 8, Zhang & Liou (1996) derived *P-T* conditions of ca.
277 760°C and minimum pressures of 2.8 GPa from an eclogite from this area, and Rolfo *et al.*
278 (2004) calculated ca. 730°C and 3.2 GPa as peak conditions recorded by a phengite-bearing
279 eclogite from the area, whereas Schmid (2000) derived maximum *P-T* conditions of ca. 4.2
280 GPa and 730°C from a phengite-bearing eclogite sampled in the nearby Changpu area. If this
281 rock had actually attained conditions above the dolomite dissociation curve, the composition
282 of magnesite can be used to estimate a minimum pressure from the shift of the reaction curve
283 in the Fe-bearing system. Fe content of dolomite decreases with increasing pressure and was

284 most likely pure $\text{CaMg}(\text{CO}_3)_2$ at the breakdown curve. Using the most Fe-rich compositions
285 of magnesite and an ideal solid solution model gives activities of ca. 0.89 for both RPC-159
286 and XU-1: this would shift the dolomite decomposition reaction to the blue curve labeled
287 $\text{mst}_{0.89}$, which is near, but not quite at the P - T estimates from eclogites.

288

289 These results are very different from what the silicates record, which re-equilibrated during
290 exhumation at pressures of around 2.5 GPa. The position of the amphibole breakdown
291 reaction can shift considerably, depending on actual mineral compositions and the intricacies
292 of the activity models used for amphibole and, to a lesser extent, for clinopyroxene and talc.
293 We used models implemented in the AX software of Holland, which are simplified at least to
294 the degree that fluorine is disregarded. The actual peak metamorphic silicate assemblage
295 stable at conditions estimated from the eclogite samples would have been clinopyroxene +
296 coesite + aragonite + dolomite/magnesite. However, only possible pseudomorphs after
297 former coesite have been found.

298

299 Mineral modes, microstructures and compositions of sample XU-1 can be explained in a very
300 similar way as for sample RPC159. The silicates preserve record of retrograde breakdown of
301 omphacite + talc to amphibole \pm quartz during decompression, indication of a prior high-
302 pressure if not ultrahigh-pressure history. Omphacite was completely consumed during this
303 reaction, and as talc is a poor container of (U)HP relics, the chance to recover UHP relics is
304 very unlikely in this type of marble. The carbonate microstructures differ from those in
305 RPC159: magnesite was apparently a stable matrix phase during much of the rocks
306 metamorphic history. Magnesite inclusions in apatite indicate that magnesite was most likely
307 present already at the beginning of the metamorphic cycle, and magnesite inclusions in
308 amphibole indicate that it was present as a stable matrix phase during amphibole growth,

309 which occurred at pressures far below the dolomite decomposition curve (Fig. 9). The modal
310 predominance of calcite over magnesite in the thin section seems to be contradictory, but
311 there is no record of primary aragonite. Quite to the contrary, all calcite is of the replacement
312 type, and the very fine grain size of the replacement products as well as the presence of
313 goethite and amorphous silica indicate that this replacement occurred at a very late (cool)
314 stage of the metamorphic history. This would corroborate conclusions drawn by Zhu *et al.*
315 (2009) that the calcite-magnesite replacement microstructures are a product of late-stage Ca-
316 metasomatism. Fe-release from decomposing magnesite at that stage might also explain most
317 of the complex compositional zoning patterns in magnesite and dolomite. The great variety of
318 calcite types indicates that two stages of magnesite replacement may have occurred: an
319 earlier one at higher temperatures producing smooth, non-porous and often compositionally
320 zoned calcite and a later one resulting in porous calcite. It is interesting to note that
321 retrogression of the eclogite also occurs in two main stages, the first one with coarse-grained
322 amphibole and clinozoisite as reaction products, and a second stage of symplectitization.
323 These stages might correlate with the magnesite replacement stages in the adjacent marble
324 and reflect events of fluid pulses passing through. Oscillatory zoned calcites in particular
325 might reflect such fluid activity.

326

327 The earlier metamorphic history of this rock is more difficult to constrain. If it was originally
328 a dolomite-magnesite marble (next to an eclogite), the reactions emanating from invariant
329 point (2) in Fig. 9 apply, and if the *P-T* estimates of Zhu *et al.* (2009) obtained from the
330 eclogite are correct, then this rock must have been outside the stability field of talc, with a
331 clinopyroxene + coesite + dolomite + magnesite peak assemblage. One possible piece of
332 evidence for that may be the only grain of quartz found in the matrix (Fig. 4a), which,
333 embedded in dolomite, may have survived the entire exhumation history. Talc would then

334 have formed as the first product of back-reaction from coesite and clinopyroxene, and may
335 have also been the first layer separating the coesite-bearing eclogite from the dolomite-
336 magnesite marble. Crossing of the degenerate reaction diopside + talc = tremolite would then
337 have replaced this layer by amphibole and consumed all matrix omphacite in the talc-
338 dominated marble. Quartz inclusions in amphibole start to react with their host during
339 exhumation according to the simplified reaction tremolite + quartz + CO₂ = talc + calcite.
340 The BSE-bright, Fe-rich goethite-SiO₂ material has also been found in this microstructural
341 setting (Fig. 6d-f), indicating that this reaction was coeval with the main stage of matrix
342 magnesite replacement. Fe²⁺ from amphibole (and not from magnesite) may have been the Fe
343 source for goethite in this case.

344

345 P-T conditions of ca. 600°C and 3.4-3.7 GPa were derived from an eclogite assemblage from
346 this outcrop and a UHP history is further corroborated by finds of coesite (Zhu *et al.*, 2009).
347 The shift of the dolomite dissociation curve calculated for this sample is again not big enough
348 (Fig. 9) to reach down to the conditions recorded in the eclogite, which could mean that the
349 aragonite + magnesite stability field had not been reached. However, it should be noted that
350 Liu *et al.* (2006) reported inclusions of aragonite and magnesite from within the “UHP-zone”
351 of a zircon, also from the same outcrop, indicating a *P-T* history that is not preserved in the
352 main mineral assemblages of marbles. It is possible that a dolomite-magnesite marble crossed
353 the dolomite dissociation curve, but that all evidence of prior aragonite produced in that field
354 was erased at least in the samples investigated by us.

355

356 Interestingly, the composition of matrix dolomites in both samples (Ca<(Mg+Fe+Mn))
357 indicates that they coexisted with magnesite rather than with aragonite; only the Ca-rich
358 “dolomite-in-dolomite” grains in sample RPC-159 seem to have Ca>(Mg+Fe+Mn). This

359 makes sense for sample XU-1, because all evidence points to a late-stage Ca-introduction into
360 the rock. In fact, these dolomite composition data corroborate the metasomatism hypothesis.
361 In the case of RPC-159, there is no evidence for Ca-transfer into the system, and the amount
362 of high-Mg matrix calcite is definitely higher than the small amount of magnesite relics (ratio
363 of at least 10:1). A possible explanation is that the composition of dolomite growing from
364 aragonite + magnesite is controlled by magnesite rather than aragonite.

365

366 **General implications**

367

368 Impure marbles have not been considered to be particularly useful for high-pressure
369 metamorphic research because most of the reactions known from simple chemical systems
370 like CaO-MgO-SiO₂-H₂O-CO₂ (CMASCH) are mainly temperature-dependent and because
371 rocks with a mixed H₂O-CO₂-fluid are not amenable to constant composition diagrams
372 (“pseudosections”). This is due to the fact that the composition of the fluid, for which the
373 system is inevitably open, changes throughout the metamorphic history in a manner that
374 becomes predictable only by including kinetic boundary conditions.

375

376 Nevertheless we have shown that the degenerate reaction tremolite = diopside + talc is a good
377 barometer that covers a certain *P-T* range because all of the minerals involved are solid
378 solutions, and it has played a central role in the *P-T* evolution of both samples investigated in
379 this study. As a degenerate reaction it is pertinent for calcite-dolomite, dolomite-magnesite
380 and pure magnesite marbles, with an increasing stability field of clinopyroxene + talc at
381 higher pressures in that sequence. Clinopyroxene-talc-marbles are replaced by clinopyroxene-
382 coesite marbles towards higher *T* and *P*, before the possible onset of dolomite decomposition.
383 The reaction of dolomite = aragonite + magnesite is again highly divariant due to variable Fe-

384 content, mainly in magnesite and dolomite, and is shifted towards lower pressures with
385 increasing Fe, becoming thus amenable for impure marbles in cold subduction zones.
386 Therefore, great care should be taken to not overlook relics of magnesite in “ordinary”
387 calcite-dolomite marbles from UHPM terrains. The role of coesite/quartz and
388 aragonite/calcite “relics” has to be evaluated carefully because both minerals can be reaction
389 products along the retrograde path, too. The role of calcite is even more critical because Mg-
390 free calcite inclusions with radial cracks might be the only criterion to derive a prior
391 aragonite + magnesite stability stage, and calcite can obviously be involved in late-stage
392 disequilibrium replacement reactions and form pseudomorphs that could be misinterpreted as
393 former aragonite.

394

395 The peak assemblage in the diamond stability field is clinopyroxene + coesite + dolomite +
396 aragonite, which is more or less equivalent to clinopyroxene + quartz + dolomite + calcite – a
397 very common assemblage at much lower pressures and higher X_{CO_2} in the fluid. Hence it is
398 also vital to search for coesite relics in “normal”-looking marbles from UHP areas.

399

400 Schertl & Okay (1994), Zhang & Liou (1996) and also the results of this study show that
401 dolomite can be good enough as a container to preserve relics such as coesite or magnesite,
402 and even talc that is no longer in equilibrium with matrix clinopyroxene. Hence, massive
403 impure marbles that have not been pervasively infiltrated by fluids during exhumation are
404 considered to preserve high-pressure relics better than metapelites, paragneisses and
405 orthogneisses, and perhaps almost as well as eclogites or metaperidotites. An additional
406 benefit in this respect is the fact that most silicate crystals are separated from each other by
407 the predominant carbonate matrix, so diffusion pathways become longer and silicate minerals
408 which are reaction partners may not come in sufficient contact by diffusion of chemical

409 species for an actual breakdown reaction to be triggered or run to completion, as in the case
410 of a fluid-consuming reaction.

411

412

413 **CONCLUSIONS**

414

415 Out of two investigated cases of magnesite-bearing impure dolomite-calcite marbles, at least
416 one has in fact attained *P-T* conditions within the magnesite + aragonite stability field. Both
417 the dolomite and the amphibole terminal breakdown reactions are highly useful
418 geobarometers for impure marbles. The microstructures and reaction histories of the
419 carbonate minerals can be quite complex and revelatory. Disequilibrium replacement of
420 magnesite by aragonite/calcite at relatively low temperatures has been observed in both
421 samples and might be common in magnesite-bearing UHP dolomitic marbles. Dolomite has
422 turned out to be a quite useful container for high-pressure relics like magnesite, talc,
423 omphacite or coesite/quartz. Impure calcite-dolomite marbles that have experienced
424 conditions in the aragonite + magnesite stability field during their earlier metamorphic history
425 may be more common than hitherto assumed. This implies *P-T* conditions that lie close to the
426 5°C/km “geotherm”, with corresponding implications for tectonic processes in these orogens.

427

428

429 **ACKNOWLEDGEMENTS:**

430

431 K. Ettinger has been very helpful in optimizing electron microprobe measurements. The first
432 author wants to gratefully acknowledge the financial support for this work by Austrian
433 Science Fund project P22479-N21.

REFERENCES

- Buob, A., Luth, R.W., Schmidt, M. & Ulmer, P. (2006): Experiments on CaCO₃-MgCO₃ solid solutions at high pressure and temperature. *American Mineralogist*, **91**, 435-440.
- Dachs, E. (1998): Petrological elementary tools for Mathematica®. *Computers and Geosciences* **24/4**, 219-235.
- Dachs, E. (2003):. Petrological elementary tools for Mathematica®; an update. *Computers and Geosciences* **30/2**, 173-182.
- Hermann, J. (2003): Carbon recycled into the deep Earth: Evidence from dolomite dissociation in subduction-zone rocks: Comment. *Geology*, **31**, e4-e5.
- Janousek, V., Farrow, C.M., Erban, V. (2006): Interpretation of whole-rock geochemical data in igneous geochemistry: introducing Geochemical data Toolkit (GCDkit). *Journal of Petrology* **47/6**, 1255-1259.
- Liu, L. & Lin, C. (1995): High-pressure phase transformations of carbonates in the system CaO-MgO-SiO₂-CO₂. *Earth and Planetary Science Letters*, **134**, 297-305.
- Liu, F.L., Gerdes, A., Liou, J.G., Xue, H.M. & Liang, F.H. (2006): SHRIMP U-Pb zircon dating from Sulu-Dabie dolomitic marble, eastern China: constraints on prograde, ultrahigh-pressure and retrograde metamorphic ages. *Journal of metamorphic Geology*, **24**, 569-589.
- Luth, R.W. (2001): Experimental determination of the reaction aragonite + magnesite = dolomite at 5 to 9 GPa. *Contributions to Mineralogy and Petrology*, **141**, 222-232.
- Martinez, I., Zhang, J. & Reeder, R.J. (1996): In situ X-ray diffraction of aragonite and dolomite at high pressure and high temperature: Evidence for dolomite breakdown to aragonite and magnesite. *American Mineralogist*, **81**, 611-624.
- Messiga, B., Kienast, J.R., Rebay, G., Riccardi, M.P. & Tribuzio, R., 1999. Cr-rich magnesiochloritoid eclogites from the Monviso ophiolites (Western Alps, Italy). *Journal of metamorphic Geology*, **17**, 287-299.
- Morlidge, M., Pawley, A. & Droop, G. (2006): Double carbonate breakdown reactions at high pressures: an experimental study in the system CaO-MgO-FeO-MnO-CO₂. *Contributions to Mineralogy and Petrology*, **152**, 365-373.
- Oberhänsli, R., Martinotti, G., Schmid, R. & Liu, X. (2002): Preservation of primary volcanic textures in the ultrahigh-pressure terrain of Dabie Shan. *Geology*, **30**, 699-702.
- Omori, S., Liou, J.G., Zhang, R.Y. & Ogasawara, Y. (1998): Petrogenesis of impure dolomitic marble from the Dabie Mountains, central China. *The Island Arc*, **7**, 98-114.
- Rolfo, F., Compagnoni, R., Wu, W. & Xu, S. (2004): A coherent lithostratigraphic unit in the coesite-eclogite complex of Dabie Shan, China: geologic and petrologic evidence. *Lithos* **73**, 71-94.

- Sato, K. & Katsura, T. (2001): Experimental investigation of dolomite dissociation into aragonite + magnesite up to 8.5 GPa: *Earth and Planetary Science Letters*, **184**, 529-534.
- Schertl, H-P. & Okay, A. (1994): Coesite inclusion in dolomite of Dabie Shan, China: petrological and rheological significance. *European Journal of Mineralogy*, **6**, 995-1000.
- Schmid, R., Franz, L., Oberhänsli, R & Dong, S. (2000): High-Si phengite, mineral chemistry and P-T evolution of ultrahigh-pressure eclogites and calc-silicates from the Dabie Shan, eastern China. *Geological Journal*, **35**, 183-207.
- Schmid, R., Romer, R.L., Franz, L., Oberhänsli, R & Martinotti, G. (2003): Basement-cover sequences within the UHP unit of the Dabie Shan. *Journal of metamorphic Geology*, **21**, 531-538.
- Zhang, L., Ellis, D.J., Arculus, R.J., Jiang, W. & Wie, C. (2003): 'Forbidden zone' subduction of sediments to 150 km depth – the reaction of dolomite to magnesite + aragonite in the UHPM metapelites from western Tianshan, China. *Journal of metamorphic Geology*, **21**, 523-529.
- Zhang, R.Y. & Liou, J.G. (1996): Coesite inclusions in dolomite from eclogite in the southern Dabie mountains, China: the significance of carbonate minerals in the UHPM rocks. *American Mineralogist*, **81**, 181-186.
- Zhu, Y-F. & Ogasawara, Y. (2002): Carbon recycled into the deep Earth: Evidence from dolomite dissociation in subduction-zone rocks. *Geology*, **30(10)**, 947-950.
- Zhu, Y-F. (2003): Carbon recycled into the deep Earth: Evidence from dolomite dissociation in subduction-zone rocks: Reply. *Geology*, **31**, e5-e6.
- Zhu, Y-F. (2005): Dolomite decomposition texture in ultrahigh pressure metamorphic marble: new evidence for the deep recycling of crustal material. *Acta Petrologica Sinica*, **21**, 347-354.
- Zhu, Y-F., Massonne, H-J., & Zhu, M-F. (2009) : Petrology of low-temperature, ultrahigh-pressure marbles and interlayered coesite-eclogites near Sanqingge, Sulu terrane, eastern China. *Mineralogical Magazine*, **73**, 307-332.

Figure and table captions

Figure 1. The most important reactions defining stability fields in the (ultra)high-pressure regime, with the 5°C/km geotherm for reference.

Figure 2. Sample RPC-159: a) coarse grained matrix omphacite and amphibole in dolomite, with quartz and calcite as early reaction products and later symplectite; b) rare relics of magnesite and talc in dolomite; c) oscillatory-zoned matrix epidote; d) detail of symplectite with fine grained, light grey diopside and coarser-grained tremolite in albite; e) rutile rimmed by retrogression titanite; f) phengitic muscovite in amphibole, decomposing to symplectite of very Ba-rich muscovite, phlogopite and albite; g) pseudomorphs of talc + calcite, possibly after former coesite, with radial cracks in omphacite; h) apatite crystals with oriented monazite exsolutions in a dolomite host.

Figure 2. Sample RPC-159: a-d) magnesite in various stages of replacement by mostly porous calcite and to a minor extent by dolomite and a porous, “talc-like” material (c); e) interstitial calcite with dolomite exsolutions; f) non-porous calcite in omphacite, with radial cracks; g) like (f), but with BSE-brighter relics of aragonite; h) BSE-brighter dolomite-2 within normal matrix dolomite, near magnesite (mostly broken out) and calcite.

Figure 3. Sample XU-1: a) coarse grained matrix amphibole and talc in dolomite, with calcite as crack fillings and pseudomorphs, and a small rounded relic of matrix quartz; b) quartz inclusions in amphibole with reaction rims of calcite + talc; c) strongly zoned dolomite with an inclusion of calcite pseudomorph after magnesite; d) magnesite with inclusions of dolomite, partly replaced by calcite; note BSE-bright Fe-rich material outlining former grain boundaries; e) detail of (c); f) omphacite relic in matrix dolomite, partly reacted to amphibole + quartz; g) zoned dolomite (detail of d).

Figure 4. Sample XU-1: calcite pseudomorphs after magnesite: a) typically with smooth rim and porous core; b) non-porous; c) non-porous with apparently euhedral magnesite inclusion; d) partly porous, smooth part zoned; e, f) with complex zoning.

Figure 5. Sample XU-1: a) magnesite inclusion in apatite; b, c) magnesite inclusions in amphibole: partly replaced by calcite (b) and fresh (c); d, e) quartz inclusion in amphibole partly replaced by talc, calcite and Fe-rich material; f) like in d) and e), but no quartz visible.

Figure 6. a) Pyroxene classification triangle showing clinopyroxene relics from XU-1 (crosses), omphacite (open circles) and symplectite diopside (dots) from RPC-159; b) Amphibole plots for Si vs. Na on the B-site, and c) Si vs. X_{Mg} for matrix amphiboles from XU-1 (crosses) and RPC-159 (dots).

Figure 7. Carbonates from XU-1 (crosses in all plots) and RPC-159 (other symbols); a) magnesite: fresh or dark parts (circles) and brighter parts (dots); b) calcite: matrix calcite (triangles), replacing magnesite (stars), non-porous calcites (circles) and aragonite (dot); c, d) dolomites: matrix dolomite (circles) and “dolomite-in-dolomite” (dots).

Figure 8. Petrogenetic grid for impure marbles in the system CaO-MgO-SiO₂-H₂O-CO₂. *P-T* conditions constrained in this and prior studies are indicated for sample RPC-159 from Dabieshan (blue) and sample XU-1 from Sulu (red): R = Rolfo *et al.* (2004), S = Schmid *et al.* (2000), ZL = Zhang & Liu (1996) and Z = Zhu *et al.* (2009). The role of the invariant points 1-4 and the pertinent reactions are explained in the text.

Table 1: Representative analyses of silicates and carbonates of samples RPC-159 and XU-1.

Figure 1

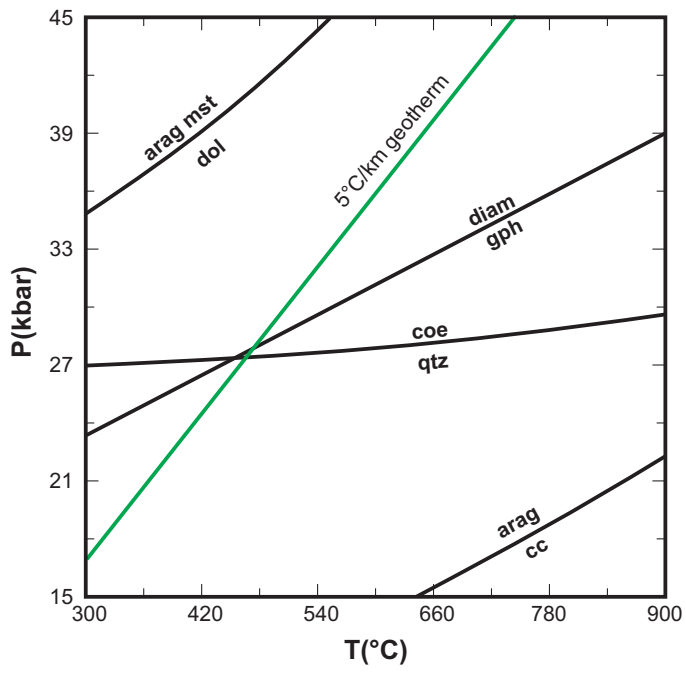


Figure 2

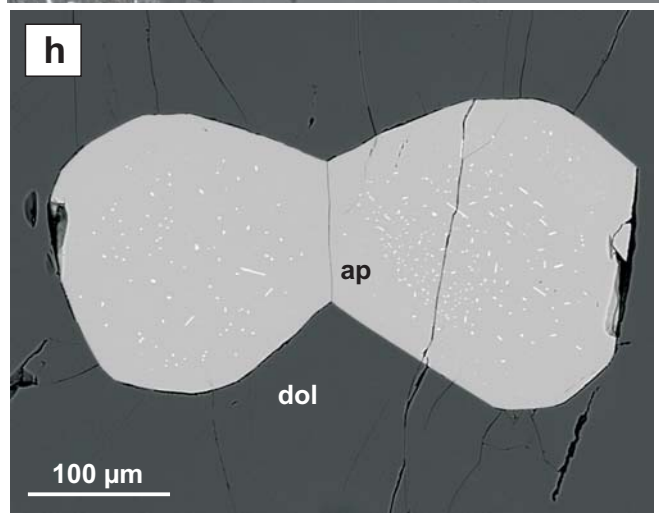
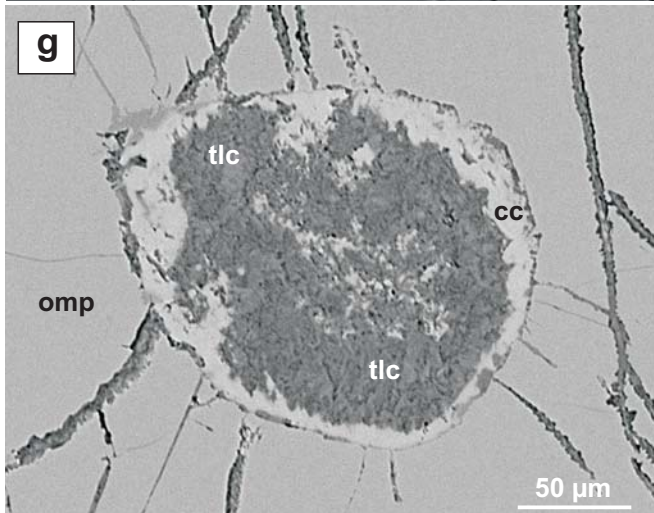
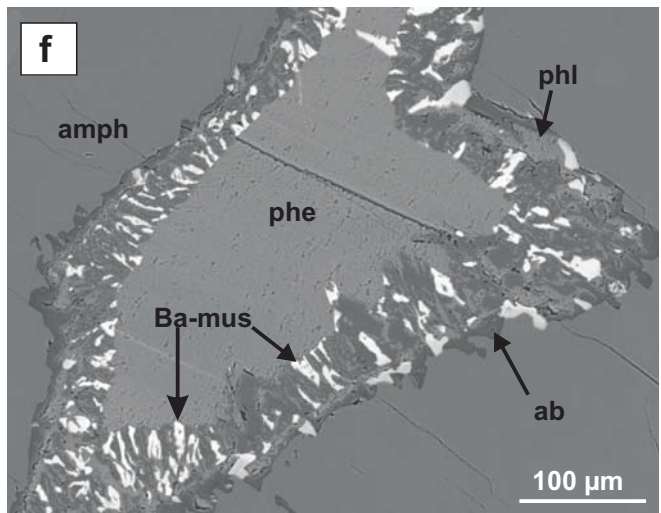
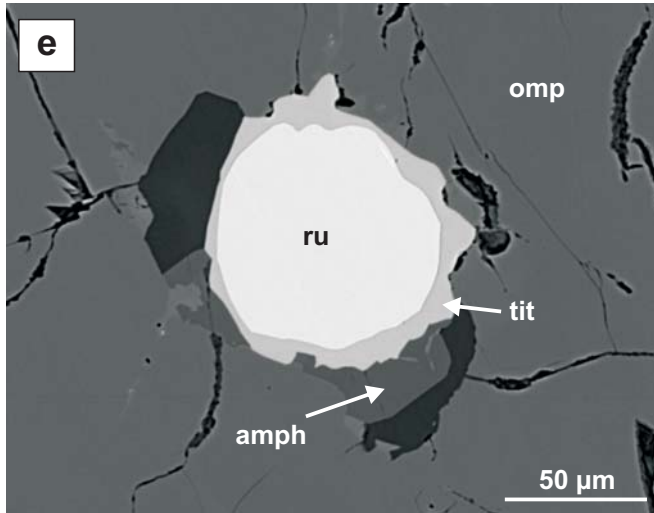
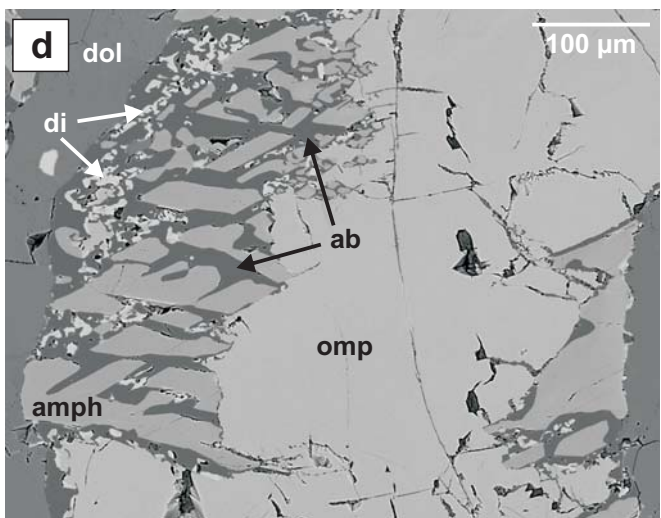
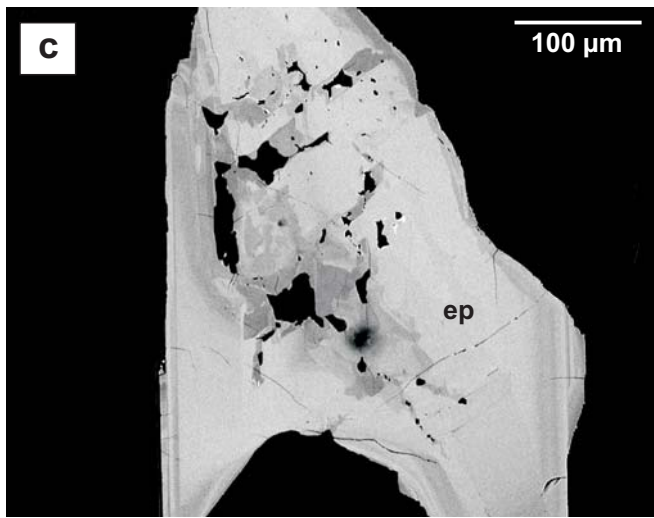
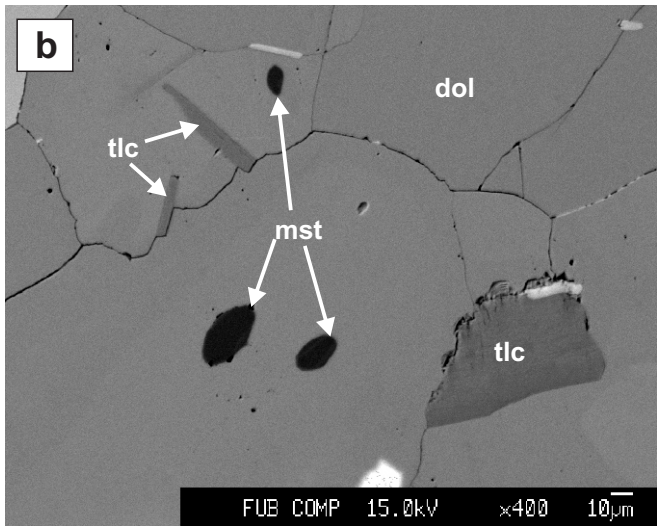
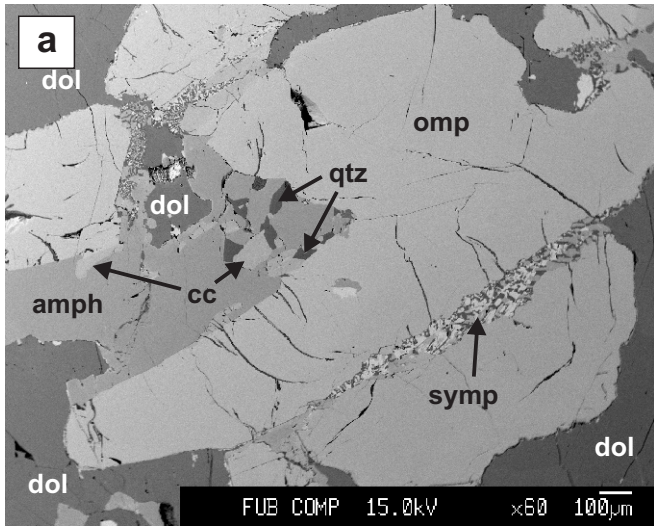


Figure 3

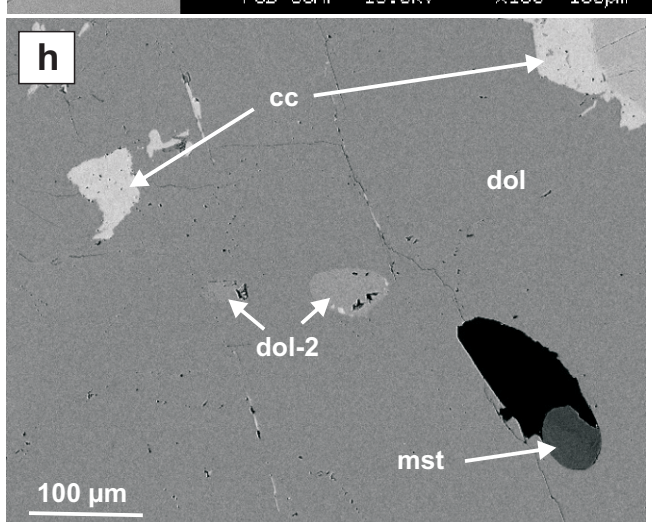
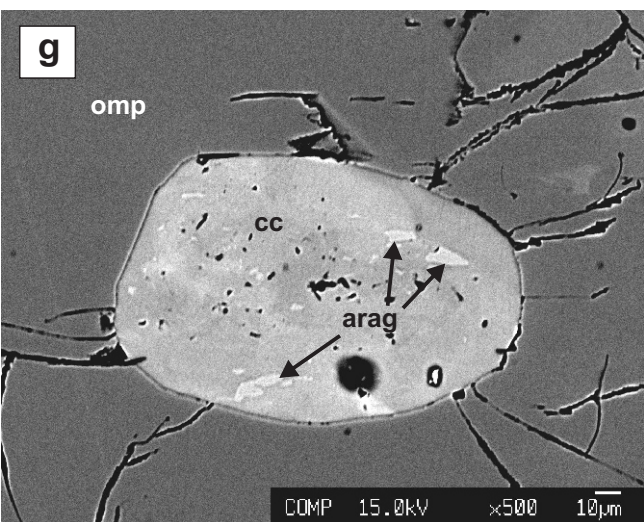
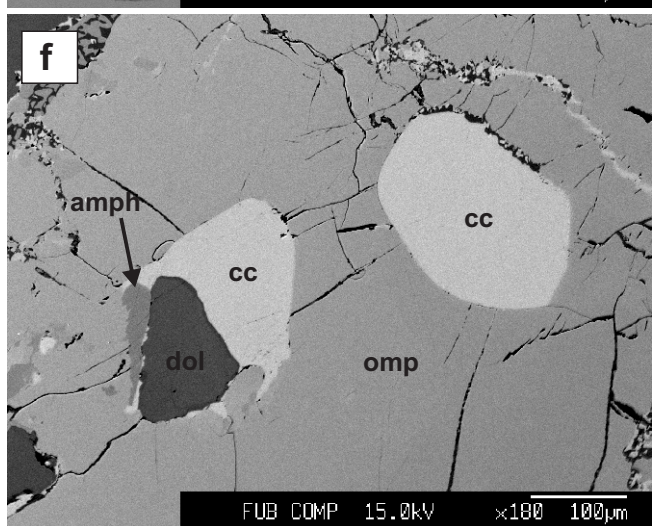
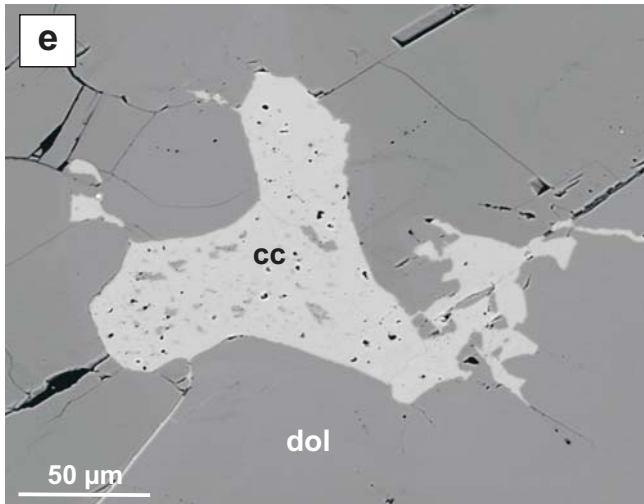
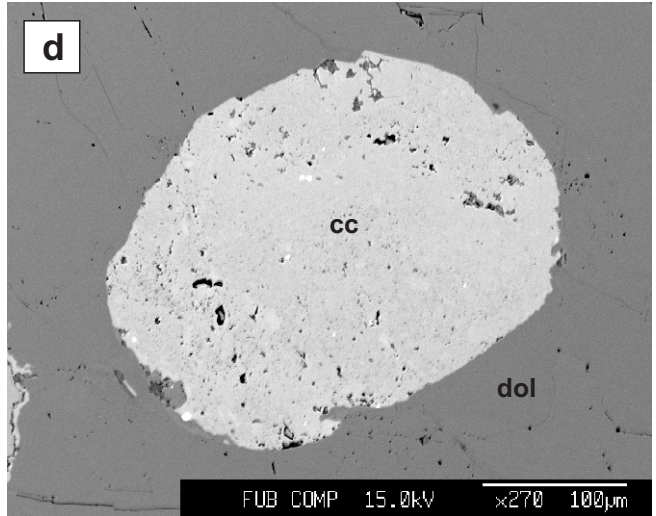
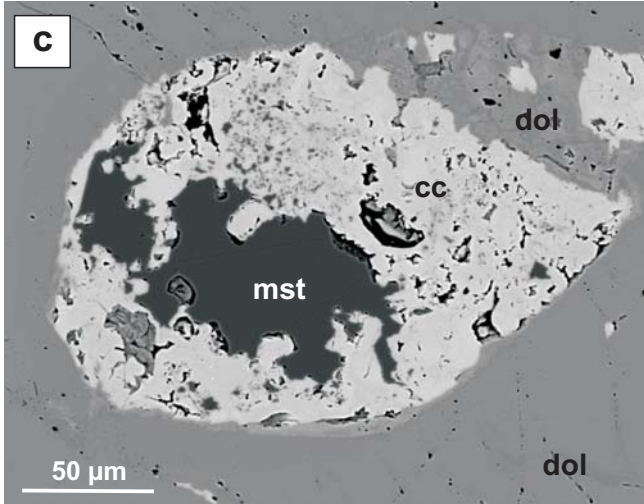
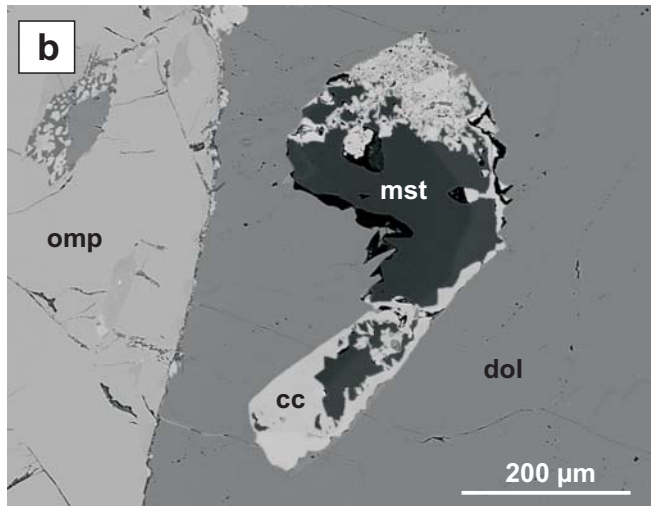
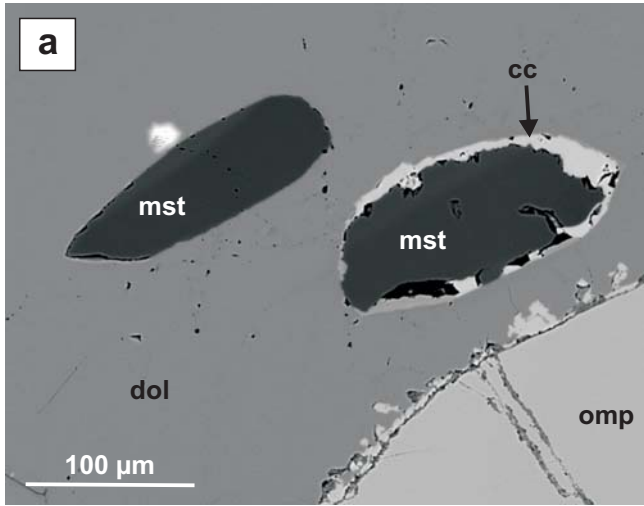


Figure 4

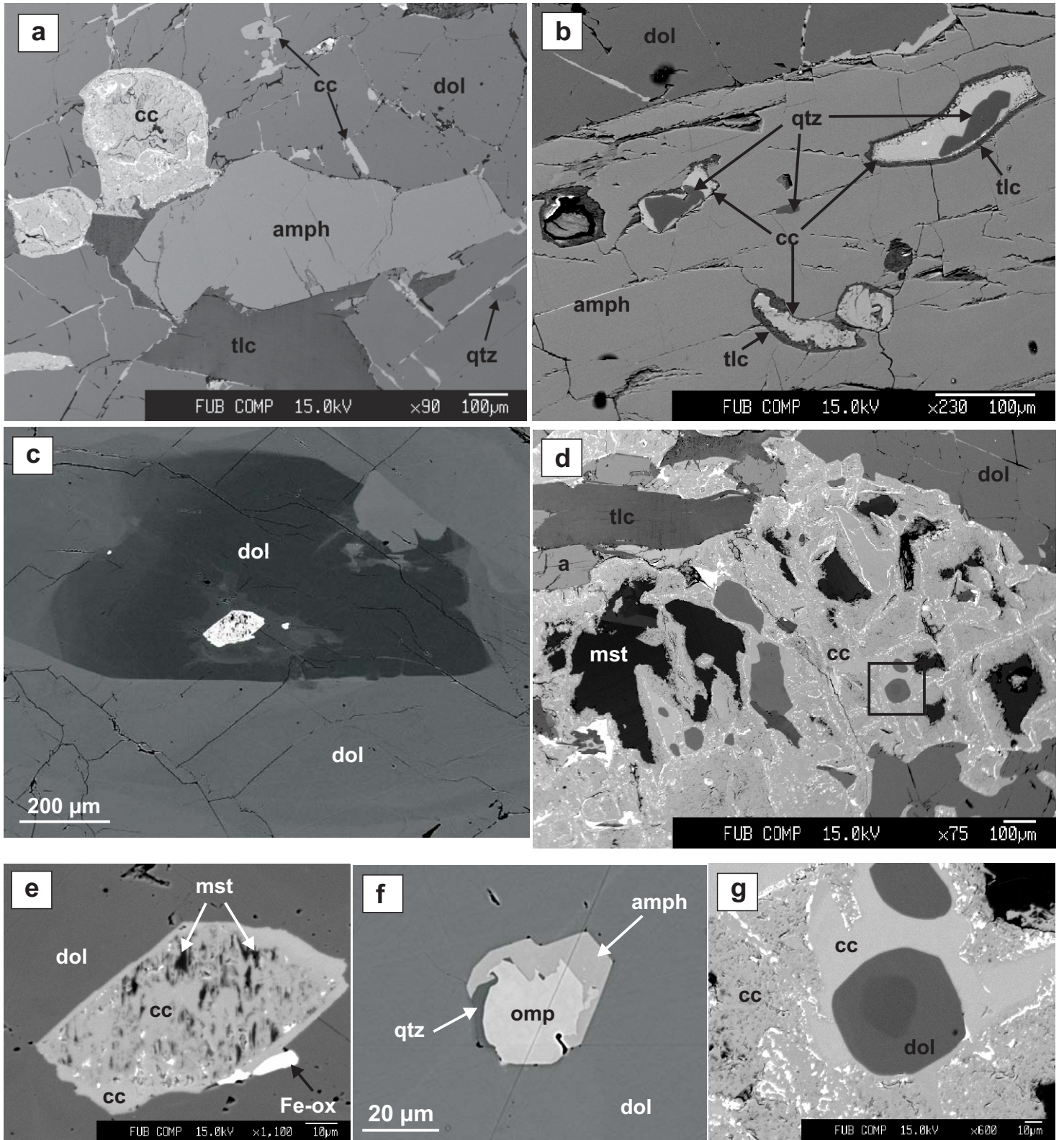


Figure 5

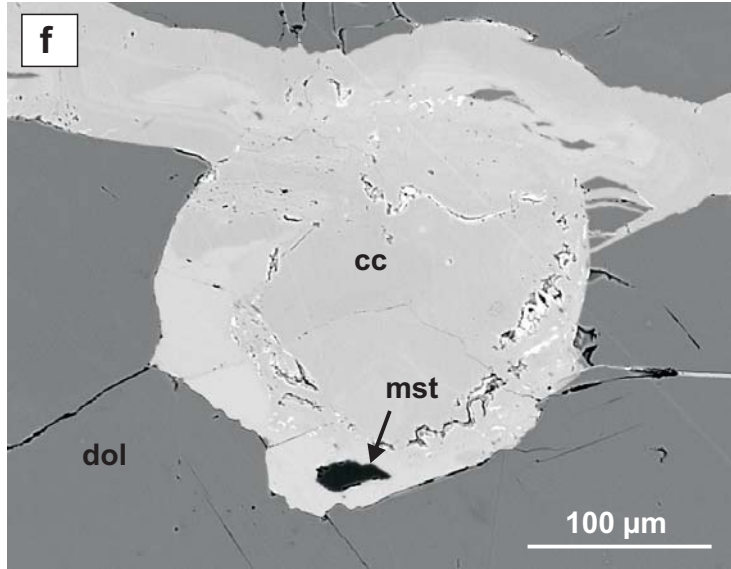
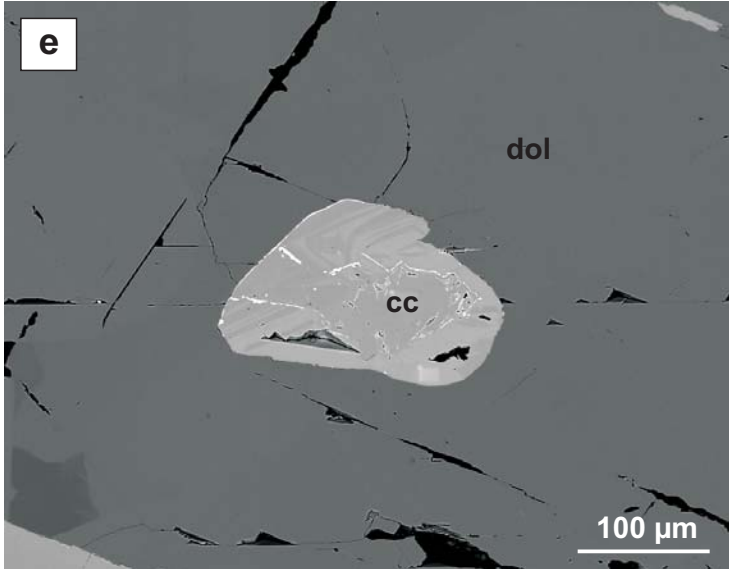
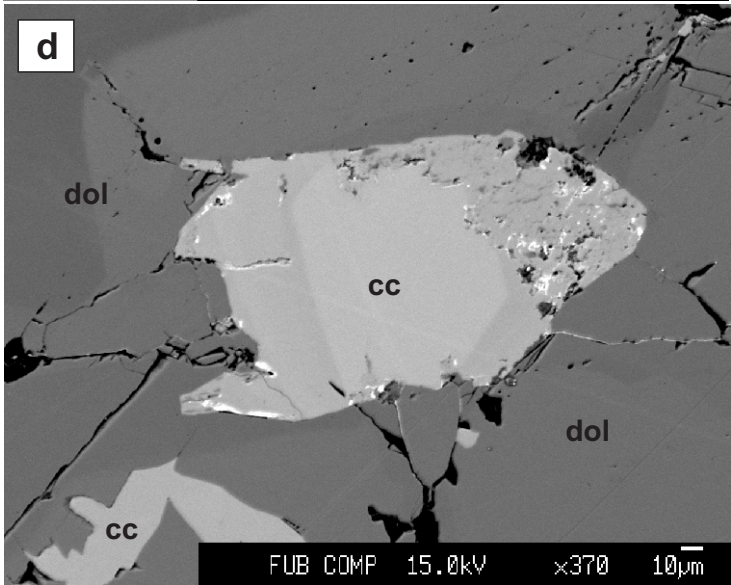
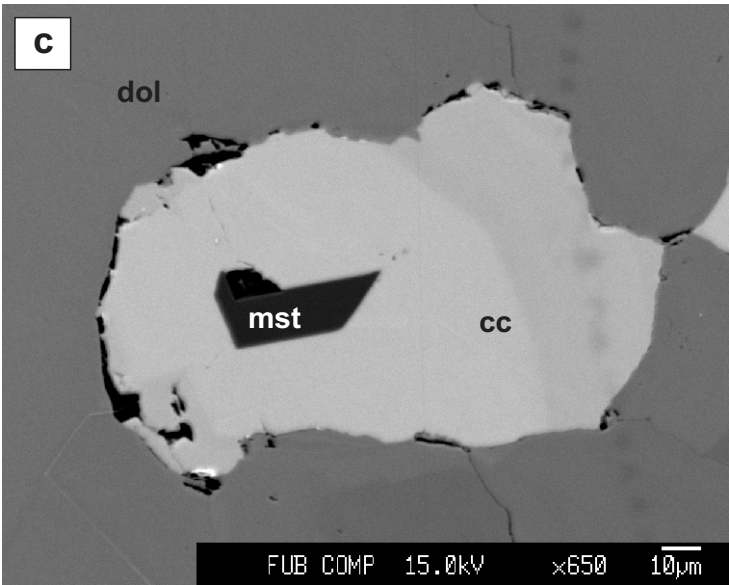
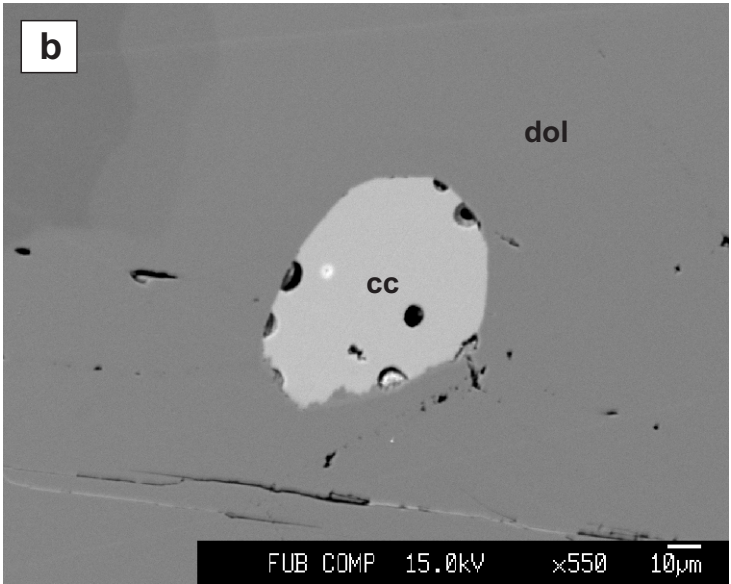
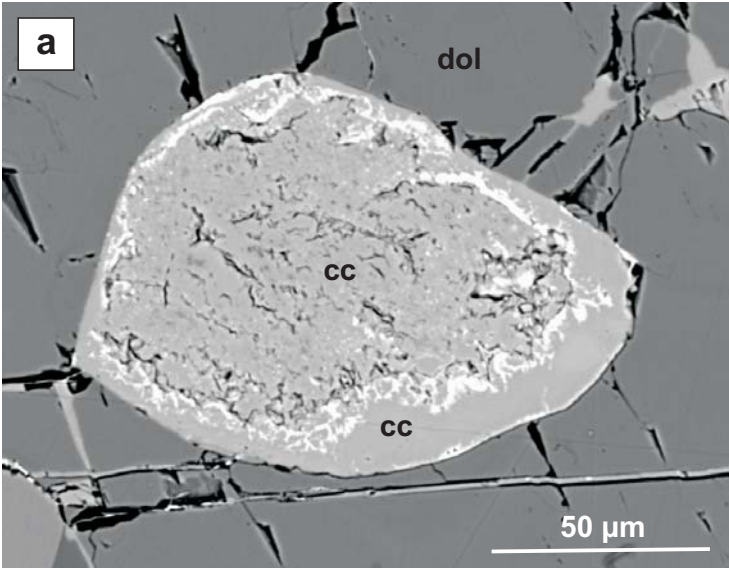
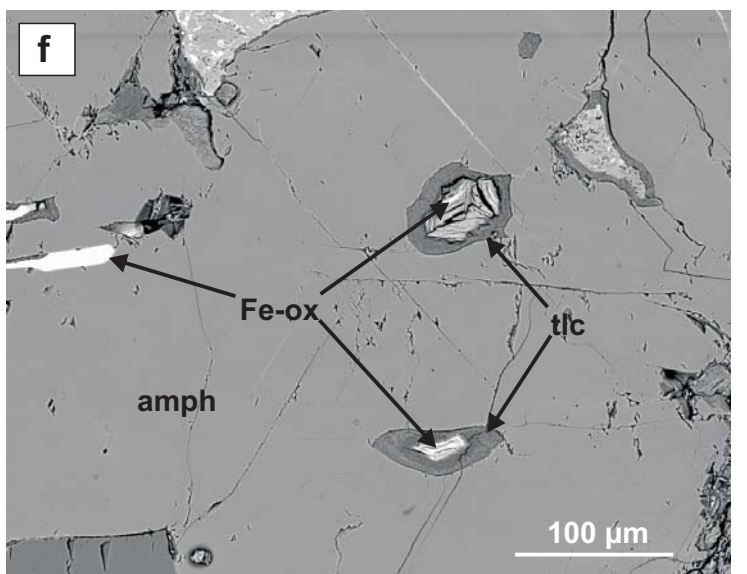
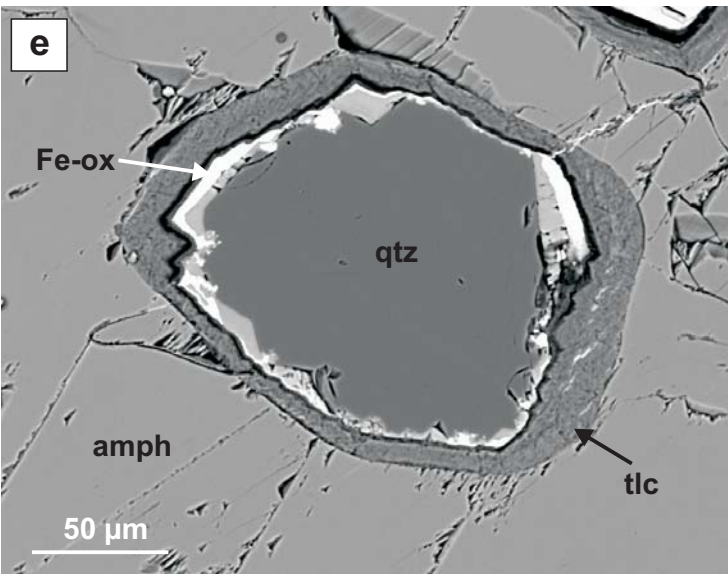
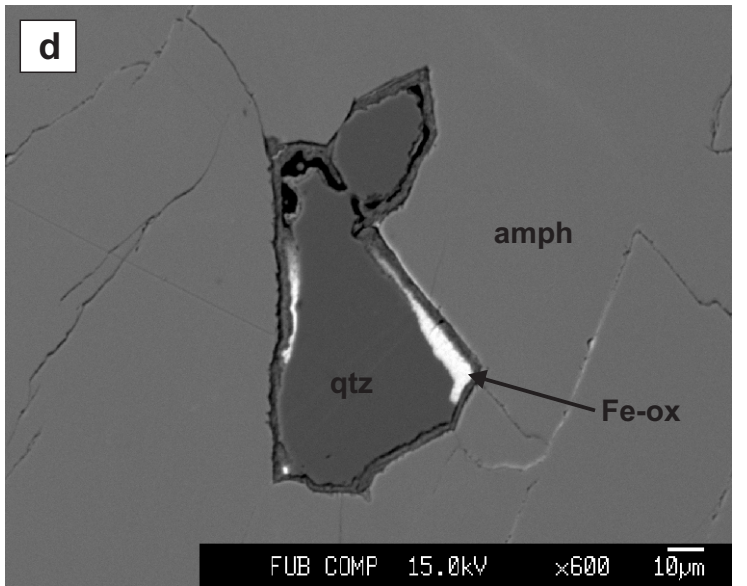
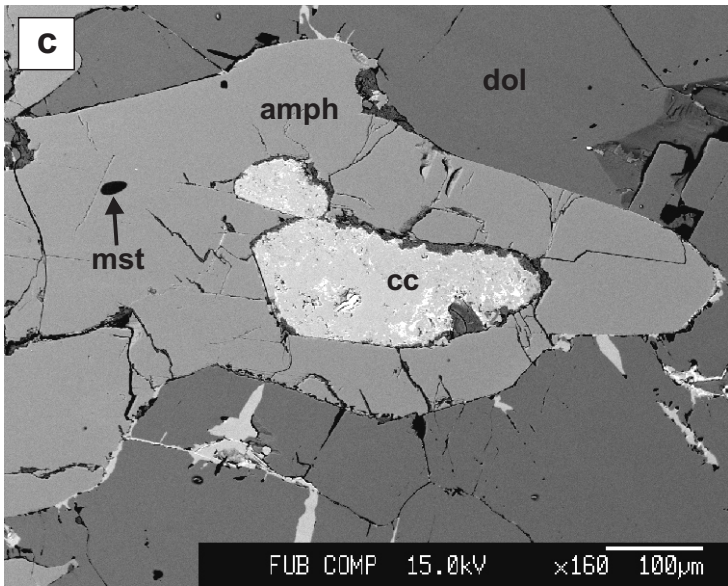
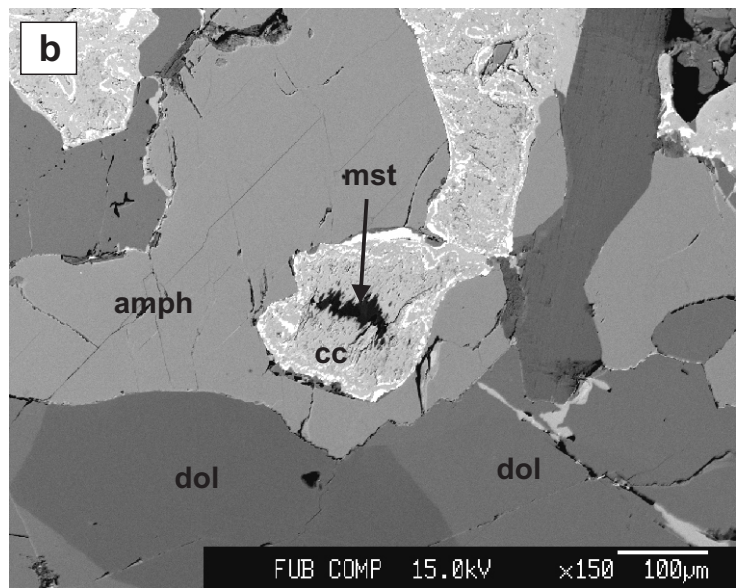
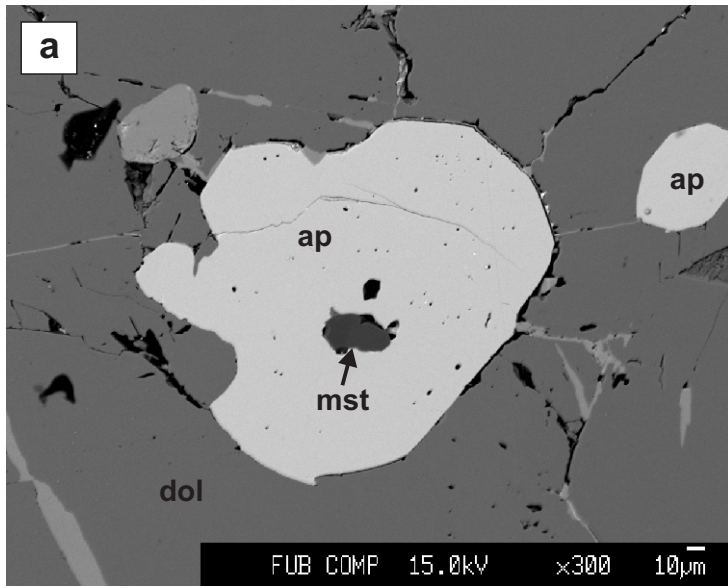


Figure 6



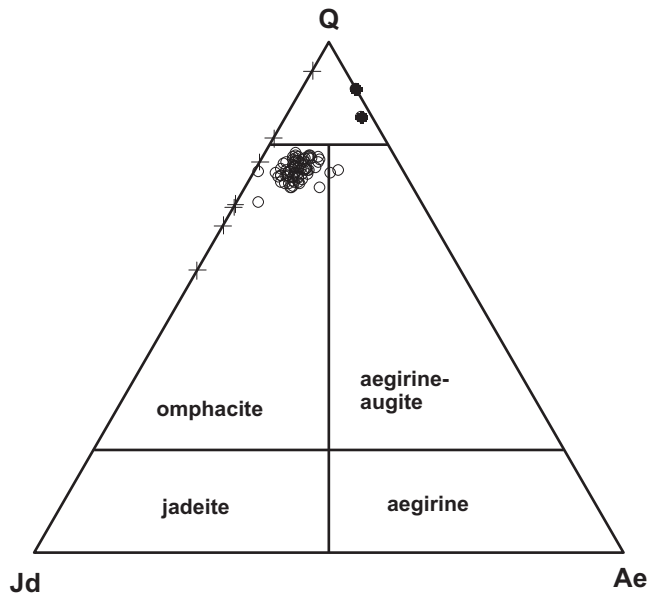


Fig. 7a

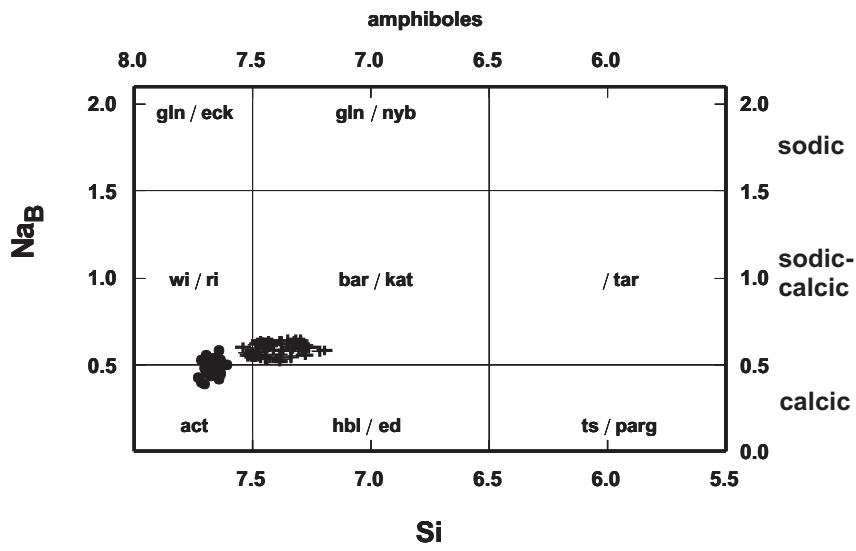


Fig. 7b

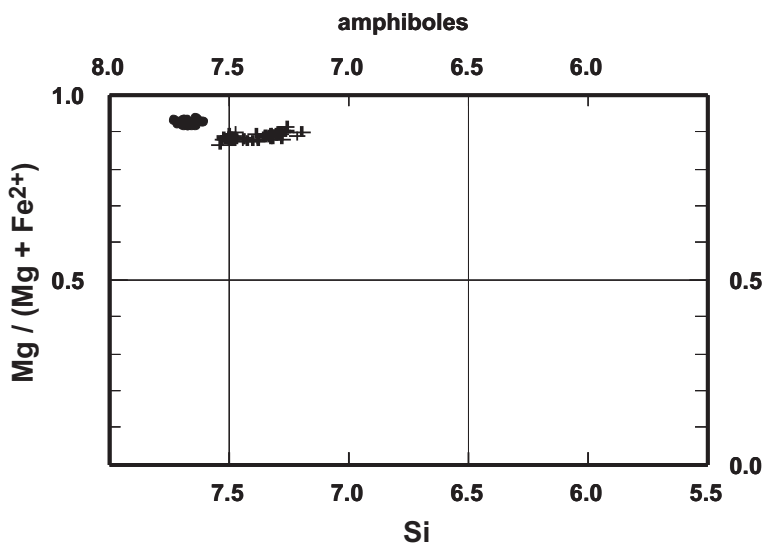


Fig. 7c

Figure 9

